Improved LAI Algorithm Implementation to MODIS Data by Incorporating Background, Topography, and Foliage Clumping Information

Alemu Gonsamo and Jing M. Chen

Abstract—Leaf area index (LAI) is one of the essential biogeophysical variables related to terrestrial carbon and biogeochemical cycles. The University of Toronto (UofT) LAI product is developed in order to support the European Space Agency GLOBCARBON project for global and climate change assessments. The climate and global change communities have recently requested for a daily 250-m LAI product in order to improve the spatial and temporal patterns of carbon pools and fluxes knowledge. In light of these considerations, we carry out further improvements on the UofT LAI algorithm, including enhanced spatial resolution (250 m) by considering an improved land cover map, local topography, clumping index, and background reflectance variations in order to produce canopy LAI time series. Here, we present the methodological framework and an evaluation of 250-m UofTv2 LAI estimates in forest stands of the Canadian Carbon Program fluxnet sites. The LAI distributions over Canada and the comparison with ground measurements show an improved LAI estimates from the UofT v2 LAI algorithm as compared with the UofT v1 LAI algorithm. One of the key differences between v1 and v2 UofT LAI product is that the former produces total LAI whereas the latter produces overstorey LAI in forest and total LAI in other vegetated land cover types. A daily LAI product can further be extracted from the 10-day UofT v2 LAI time series by fitting various curve fitting algorithms. Although, we have shown the LAI product only over Canada, the algorithm can also be extended for a global 250-m LAI product.

Index Terms—Clumping index, geometrical-optical model, leaf area index, MODIS, University of Toronto (UofT) leaf area index (LAI) algorithm.

I. Introduction

VEGETATION plays a major role in global physical and biogeochemical processes by strongly regulating gas and matter exchanges between the terrestrial biosphere and the atmosphere. To predict future climate change accurately and find ways to manage the concentration of atmospheric carbon dioxide, the processes and feedbacks that drive the terrestrial carbon cycle must first be understood. Our current knowledge of spatial patterns of carbon pools and fluxes is uncertain, particularly over land although good results were obtained on

The authors are with the Department of Geography and Program in Planning, University of Toronto, Toronto, ON M5S 3G3, Canada (e-mail: gonsamoa@geog.utoronto.ca; chenj@geog.utoronto.ca).

global carbon balance [1]. Global vegetation cover dynamics, such as deforestation, reforestation, aforestation, and seasonal agriculture is patchy and only if space-based surface biogeophysical observations are operating on a similar spatial scale, one can clearly identify changes in carbon storage over time and minimize sampling errors due to spatial aggregation. Regional carbon budget models, such as the carbon budget model of the Canadian forest sector (CBM-CFS) [2] are based on irregular forest inventory polygons requiring gridded spatial datasets at higher resolution to reduce sampling and spatial matching errors with other regularly gridded results. It has been shown that the optimal spatial resolution for satellite-based climate variables, such as land cover maps, fraction of absorbed photosynthetically active radiation (fAPAR), leaf area index (LAI), lake area, and fire disturbance products should be at moderate resolution of ∼250 m in order to correctly describe the spatial heterogeneity of the land surface [3]. The spatial Fourier analysis conducted by [3] over North America's typical agricultural area shows that, in addition to a strong signal at very small scales, there exist two maxima at 200–300 m and 400–700 m scales, which describe the typical size of various land cover types. Therefore, for regular gridded aggregation of regional carbon models, such as CBM-CFS over Canada, irregular forest polygons can be resolved more accurately at ∼250-m spatial resolution.

One of the essential climate biogeophysical variables identified by the global climate observing system (GCOS) [4] related to terrestrial ecosystems and supported by space-based earth observations for climate change assessment, mitigation, and adaptation is LAI. LAI is defined as one half of the total leaf surface area per unit ground surface area projected on the local horizontal datum [5] and [6]. Various national and international projects, such as the NOAA/AVHRR [7], ECOCLIMAP [8], CYCLOPES [9], University of Toronto (UofT GLOBCARBON) [10], TERRA-AQUA/ MODIS [11], and one regional product produced by the Canada center for remote sensing (CCRS) over Canada [12] provide regional- and global-level estimates of LAI and other land surface parameters. Recent intercomparison studies among these LAI products, have pointed out that the UofT LAI GLOBCARBON product successfully captures realistic and consistent seasonal and interannual LAI variability of most land covers with large LAI dynamic ranges [13], [14]. However, it has also been indicated that the UofT GLOBCARBON LAI products perform poorly in mountainous areas and may have inadequately

been represented for land cover variation by Global Land Cover 2000 (GLC2000) product. In most global products, subpixel heterogeneity has been a source of uncertainty related to scaling error due to prevailing small patches of vegetation in contrast to coarser resolutions of the LAI products. In addition to this, GCOS has specified a requirement for global daily ~250-m resolution LAI estimates with a total error of less than 10%. Therefore, in this paper, we present a contribution to the UofT LAI algorithm initiative by improving the spatial resolution, employing an enhanced land cover map from the same satellite instrument and considering spatially explicit local topography, clumping index, and background reflectance variations in order to produce an improved canopy LAI time series.

II. METHODOLOGY

A. Overview of the UofT LAI Algorithm

Deng *et al.* [10] produced the UofT LAI algorithm based on the four-scale geometrical optical model [15] with a multiple scattering scheme [16]. The algorithm makes use of the four-scale simulations characterized by the relationship between LAI and the bi-directional reflectance distribution function (BRDF) of red (ρ_R), near infrared (NIR: ρ_{NIR}), and shortwave infrared (SWIR: ρ_{SWIR}) reflectances for each distinctive land cover type. The BRDF property is represented by the view-target-sun geometries: view zenith angle (θ_v), sun zenith angle (θ_s), view azimuth angle ($\varnothing_v$), and sun azimuth angle ($\varnothing_s$). The land cover types with similar structural characteristics are combined to form six biomes based on canopy architecture–needleleaf forest, tropical forest, broadleaf forest, mixed forest, shrub, and cropland and grassland. Nonvegetated land and water surfaces are assigned an LAI value of zero. The LAI is retrieved from a lookup table (LUT), which is, in turn, generated from the BRDF of the three spectral bands producing simple ratio (SR $= \rho_{NIR}/\rho_R$) and reduced simple ratio (RSR $= \rho_{NIR}/\rho_R (1 - \rho_{SWIR} - \rho_{SWIRmin}\rho_{SWIRmax} - \rho_{SWIRmin})$) vegetation indices based on the interactions of incidence solar radiation and the vegetated surface represented by an *a priori* range of ancillary parameters (e.g., land cover types, soil and leaf optical properties, canopy shape and height, and foliage element clumping index at the plant and canopy scales). The RSR is used for the retrieval of LAI for forest land cover, whereas SR is used for other vegetated land cover, as follows:

$$\text{LAI}_\text{forest} = f_{\text{LAI}_{\text{RSR}}}\left[\text{SR} \cdot f_{\text{BRDF}}\left(\theta_v, \theta_s, \phi_v - \phi_s\right) \right. $$
$$\left. \times \left(1 - \frac{\rho_{\text{SWIR}} \cdot f_{\text{SWIR}_{\text{BRDF}}}\left(\theta_v, \theta_s, \phi_v - \phi_s\right) - \rho_{\text{SWIRmin}}}{\rho_{\text{SWIRmax}} - \rho_{\text{SWIRmin}}}\right)\right] $$

(1)

and

$$\text{LAI}_\text{others} = f_{\text{LAI}_{\text{SR}}}\left[\text{SR} \cdot f_{\text{BRDF}}\left(\theta_v, \theta_s, \phi_v - \phi_s\right)\right] \quad (2)$$

where LAI_forest is LAI value retrieved for forest land cover, and LAI_others is LAI value retrieved for other vegetated land cover types. ρ_{SWIRmax} and ρ_{SWIRmin} are the maximum and minimum SWIR reflectances selected for specific land covers types, respectively. $f_{\text{BRDF}}(\ )$ and $f_{\text{SWIR}_{\text{BRDF}}}(\ )$ are the BRDF

modification functions for SR and SWIR reflectance, respectively, derived from a modified two-kernel Roujean's model [17] corrected for pronounced hotspot effect [18]. $f_{\text{LAI}_{\text{SR}}}[\ ]$ and $f_{\text{LAI}_{\text{RSR}}}[\ ]$ are functions describing the relationships between BRDF-modified SR and RSR with LAI, respectively. These functions, including the kernel coefficients for converting reflectances and SR from one angle to another are fitted with Chebyshev polynomial of second kind. Details of the shape-based land cover-specific BRDF kernel coefficient determination and computational methodologies for a large-scale LAI inversion are given in [10].

The LAI retrieved from (1) and (2) is inverted assuming a random distribution of foliage elements in space; therefore, resulting in "effective LAI" [19]. The final "true LAI" is obtained from dividing the effective LAI by foliage element clumping index [19], which is also included in the UofT LAI algorithm process scheme. After all these processes, the retrieved LAI can still be contaminated by atmospheric effects, missing and bad quality reflectance measurements, which are characterized by erratic temporal LAI trends. To minimize these effects, the UofT LAI algorithm uses an approach to reconstruct the possible seasonal trajectory of LAI time series based on a series of cubic spline curves. This approach fits the locally adjusted cubic-spline capping (LACC) function; therefore, optimum local smoothing coefficients are assigned to every 10-day LAI value based on the curvature of the initially fitted curve with an average global smoothing coefficient [20].

The UofT v1 LAI algorithm, as originally presented in [10] and used to retrieve regional and global LAI, including the generation of GLOBCARBON product [13] and [21] uses an empirical and land cover-dependent clumping index; does not consider topographic variation as often overlooked in global, regional, and *in situ* land remote sensing products [22], [23]; and assumes fixed background reflectances having constant values across pixels and land cover types. In the following sections, we present the improvements made in the UofT LAI algorithm. Although the improved LAI retrieval method discussed hereafter was optimized for global applications, this paper presents a Canada-wide product. Fig. 1 presents a flowchart of the steps followed to improve the UofT LAI product. The main improvements of v2 over v1 are consideration of a spatially explicit pixel-by-pixel: 1) clumping index; 2) local topography; and 3) background reflectances with improved normalization of their contribution on canopy LAI. The UofT v1 LAI algorithm produces total LAI values, i.e., LAI of both overstorey and understorey since the fixed background value as used in v1 [10] was only for typical soil reflectances. Whereas the UofT v2 LAI algorithm is aimed to produces canopy (overstorey) LAI in forest and total LAI in other vegetated land cover types.

B. Consideration of Terrain Topography

In the UofT v1 LAI algorithm, the BRDF properties are represented by the view-target-sun geometries: θ_v, θ_s, $\varnothing v$, and $\varnothing s$. The recent validation reported that the algorithm performed poorly in hilly areas, such as the Rocky Mountains

of Western Canada [13], [21]. Note that the UofT LAI algorithm takes into consideration the BRDF effects (e.g., Fig. 1 [10]). In hilly areas, it is important to consider the view and sun incidence angles to local terrain instead of the view and sun zenith angles to horizontal datum. Under conditions of a constant view-target-sun geometry, the view and sun incident angles relative to the normal to a sloping surface would be different from those of a horizontal surface. The new BRDF indicating the relative sun and view incident angles can be represented as a "slope-surface-BRDF." To this effect, new sets of view and sun incidence angles, (γ_v) and (γ_s), respectively, were calculated using a digital elevation model (DEM) as follows:

$$\gamma_v = \arccos\left[\cos\theta_v \cos\beta + \sin\theta_v \sin\beta\cos(\phi_v - \phi_t)\right] \quad (3)$$

and

$$\gamma_s = \arccos\left[\cos\theta_s \cos\beta + \sin\theta_s \sin\beta\cos(\phi_s - \phi_t)\right] \quad (4)$$

where β and ϕ_t are the terrain slope and azimuth angles, respectively. The DEM is obtained from the Canadian digital elevation data (CDED) (ftp://ftp2.cits.rncan.gc.ca/pub/geobase/official/cded/). The digital source data for CDED at scales of 1:250 000 (3–12 arc sec) were extracted from the hypsographic and hydrographic elements of the national topographic database and various scaled positional data acquired from the provinces and territories. The β and ϕ_t were derived from the DEM after resampling and reprojecting based on the nearest neighbor into 250-m resolution using the Lambert Conic Conformal projection to match the MODIS data.

The new computational searches for slope-surface-BRDF versus LAI relationships can be expressed as

$$\text{LAI}_{\text{forest}} = f_{\text{LAI}_{\text{RSR}}}\Bigg[\text{SR} \cdot f_{\text{BRDF}}\left(\gamma_v, \gamma_s, \phi_v - \phi_s\right)$$
$$\times \left(1 - \frac{\rho_{\text{SWIR}} \cdot f_{\text{SWIR}_{\text{BRDF}}}\left(\gamma_v, \gamma_s, \phi_v - \phi_s\right) - \rho_{\text{SWIRmin}}}{\rho_{\text{SWIRmax}} - \rho_{\text{SWIRmin}}}\right)\Bigg]$$
$$(5)$$

and

$$\text{LAI}_{\text{others}} = f_{\text{LAI}_{\text{SR}}}\left[\text{SR} \cdot f_{\text{BRDF}}\left(\gamma_v, \gamma_s, \phi_v - \phi_s\right)\right] \quad (6)$$

where unlike (1) and (2), the functions, $f_{\text{LAI}_{\text{SR}}}[]$ and $f_{\text{LAI}_{\text{RSR}}}[]$, are defined as functions describing the relationship of LAI with slope-surface-BRDF SR and RSR, respectively, whereas $f_{\text{SWIR}_{\text{BRDF}}}()$ and $f_{\text{BRDF}}()$ are functions describing the relationship between slope-surface-BRDF modification function for SWIR reflectance and SR, respectively. In addition to these, the view and sun zenith angles are replaced by view and sun incidence angles.

The proposed terrain topography consideration assumes uniform slope of a given pixel, similar to the commonly used topographic correction methods for surface reflectances based on view-target-sun geometries. The drawback of all these topographic correction methods is that in a complex terrain, such as gully and ridges at subpixel scale, the terrain effect cannot be fully corrected. Shadows cast by the surrounding terrains also cannot be removed. Across Canada sloping terrains mostly occur in forested regions, mostly in Rocky

Mountain forests in Western Canada. On sloping ground, tree trunks typically grow straight up, branches grow to give the most leaves the most light, which may not follow the same microscale terrain relief giving rooftop architecture of forest canopy along the hillyslopes. Therefore, the appropriate scale for the correction is hillslope scale. The primary level of radiative interaction in forests is within tree canopies. For LAI retrieval from optical remote sensing measurements, absorption by chlorophyll and leaf volume scattering the latter governed by the path length across the photosynthetic biomass are the key sources of information. The average path length of a ray of light traversing through forest canopy varies with hillslope geometry relative to sun geometry. This results in, for example, lower values of SR and RSR for hillslopes facing sun compared to flat terrain due to shorter path length and consequently lower leaf scattering within tree canopies. Our approach of terrain topography consideration therefore assigns the correct view-target-sun geometries at hillslope scale, and does not correct subpixel terrain effects and shadows cast by surrounding terrains.

C. Other Improved Input Dataset

1) 250-m Reflectance Measurement: The 250-m MODIS clear sky 10-day top of atmosphere (TOA) reflectance composites produced at the CCRS in Lambert Conic Conformal projection [24] were used instead of the standard MODIS MOD09 reflectance products. The UofT LAI algorithm relies on vegetation indices based on a shortwave infrared (SWIR) reflectance to retrieve LAI over forest targets as this reduces errors due to aerosol variability and differences in foliage types [10], [12]. Therefore, we were not able to directly use the MODIS surface reflectance product MOD09 (available at: http://modis-land.gsfc.nasa.gov/surfrad.htm) produced by the MODIS science team as SWIR reflectance data are only available at 500-m resolution. Details on spatial downscaling of SWIR reflectance from 500 to 250 m, reprojection and normalization of generated 250-m images to original 500-m images to preserve radiometric and spectral consistency are given in [24]. The red and NIR CCRS 10-day composites also differ from the standard MOD09 products by clear sky compositing technique. The 10-day composites are made based on a method developed at CCRS to produce the mask of clear-sky, cloud, and cloud shadow at 250-m resolution by employing a scene-dependent decision matrix compositing scheme, which was proven to result in a better product compared to the standard MODIS product [25]. However, it is possible to use both UofT v1 and v2 LAI algorithms with standard MODIS products given that the SWIR is interpolated into 250 m for the 250-m LAI product or directly the standard MODIS 500- and 1000-m data for a coarser LAI products. The CCRS 250-m MODIS clear sky 10-day reflectance composites used hereafter in the UofT LAI algorithms include all available ranges of pixel qualities and flags, meaning there was no pixel quality filtering prior to LAI retrieval. The retrieved LAI instead goes through the UofT LAI post processing scheme, involving the temporal smoothing of LAI time series (Fig. 1).
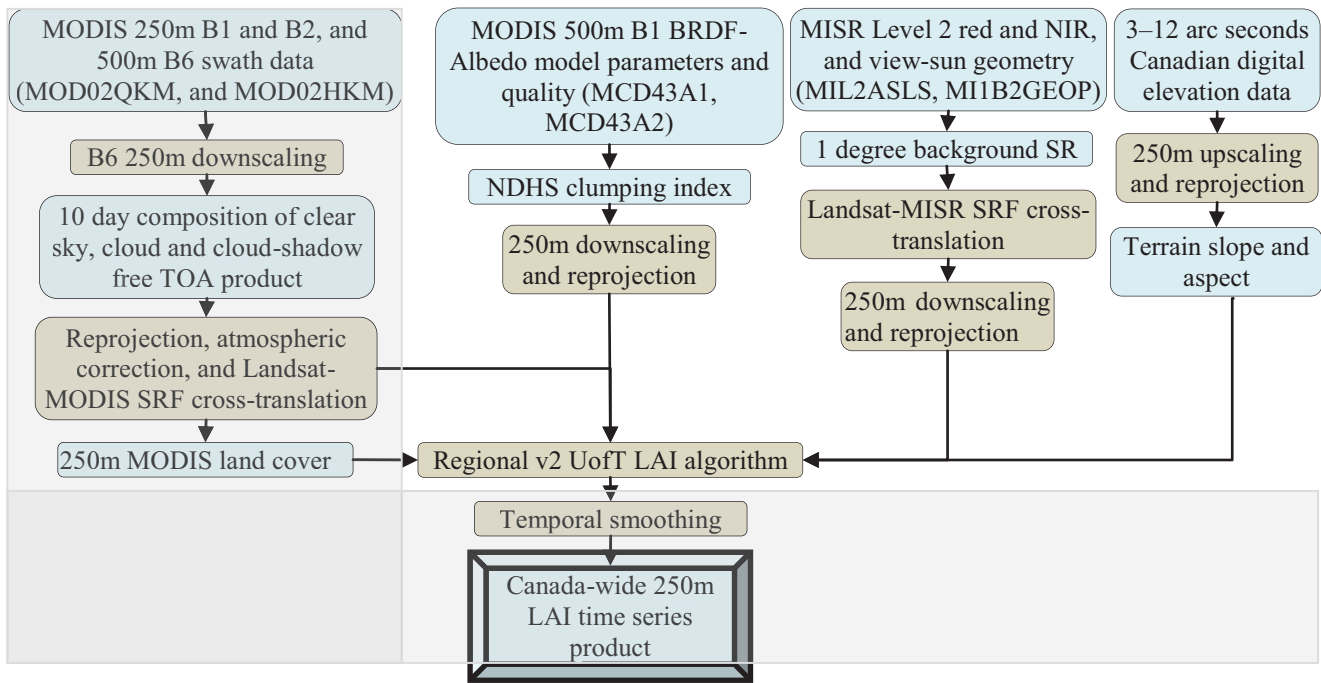
Fig. 1. Flowchart of the steps followed to improve the UofT LAI product time series. The grey shades indicate the processing scheme required for the UofT v1 LAI product.

The red, NIR and SWIR reflectances were further post-processed to match the UofT LAI algorithm. The post-processing includes fitting the spectral response function (SRF) from MODIS into Landsat 7 enhanced thematic mapper plus (ETM+) central bands for which the UofT LAI LUT was generated [26]. Prior to adjusting the SRF, the CCRS TOA data were atmospherically corrected in order to produce the top of canopy (TOC) reflectance as follows. Given that the TOA was generated based on 10-day composites for the entire spectral and spatial domain, it is fair to assume that the atmospheric interference is the lowest after the compositing, making it unnecessary to perform Canada-wide pixel-based atmospheric correction. Further, the SRF of MODIS TOA was cross-calibrated to that of the surface reflectance of ETM+ band in order to make the modified UofT LAI algorithm feasible for commonly available MODIS TOA composite data in further LAI production. This was accomplished based on TOA simulated using a combination of the 6S atmospheric model [27] and the physically based four-scale geometrical optical model [16] comprising large ranges of land cover types, soil and leaf optical properties, canopy shape and height, foliage element clumping index, and view-target-sun geometries. We have used 6S to simulate the TOA from four-scale outputs using the continental aerosol model with an aerosol optical depth (AOD550 nm) value of 0.06. Assuming the highest atmospheric transparency, water vapour (C_{H2O}, g·cm^{-2}) and ozone (C_{O3}, DU) were set to 0.419 and 480, respectively, for their column-integrated concentrations. For red and NIR, the cross-calibration of SRF between MODIS TOA and ETM+ TOC was based on ordinary least-squares (OLS) regression model using red, NIR and SR as regressors. For SWIR, the cross-calibration was based on band-to-band OLS regression model. Both SRF cross-calibrations resulted in statistically significant fit. Both SRF cross-calibration approaches were found based on several attempts following the results of [26].

2) 250-m Land Cover Data: Although the implementation of the UofT LAI algorithm can be done using any regional or global land cover products, the 1-km Global Land Cover (GLC2000) product used in UofT v1 LAI retrieval has been found to be unsatisfactory for some land cover types [29]. In this paper, we have used the 2005 North American Land Cover (NALC2005, http://www.cec.org/), which is derived from the same sensor as the LAI input (250–500-m MODIS data) at 250-m resolution. In-house analysis indicated that the GLC2000 has underestimated the Canadian forest cover by 500 000 km^2 compared to the NALC2005 and National Forest Inventory estimates over Canada. The 2005 MODIS-based land cover product has shown better accuracy compared to GLC2000 [28]. The use of NALC2005 land cover product will minimize land cover-based biases, originating from land cover-based parameterization, pixel misregistration, and coarser pixel resolution encountered in GLC2000. The burn areas are updated by replacing 2005 burn with nearest nonburn, nonwater, nonurban, or nonwetland land covers and by adding the concurrent burns from monthly MODIS Collection 5 Burned Area Product (MCD45) derived from MODIS Aqua and Terra datasets.

3) Background Reflectance Data: The spectral signatures of the background vary geographically as well as temporally with season. In forests, the background may include understorey shrub and grass, green moss, litter, rock, snow, soil, etc, which are illuminated and visible from above. The impact of the background on canopy reflectance further depends on the amount of overstorey foliage and incidence view-target-

sun geometry. The smaller view or sun incidence angles, the more background impact on canopy reflectance or vice versa. The inclusion of seasonally and spatially variable forest understory information into the LAI algorithm is, therefore, highly desirable. In the UofT LAI algorithm, the impact of the background reflectance is represented by its SR value (SR_b). Pisek and Chen [29] produced a one-degree monthly forest background brightness dataset over North America using Multiangle Imaging Spectroradiometer (MISR) data. For current LAI algorithm improvement, we have incorporated the MISR-derived SR_b into the LAI algorithm. The incorporation is made through including the bi-directional contribution of background SR represented by the gap fraction and view-target-sun incidence geometry (7) rather than the actual view-target-sun zenith geometry. Pisek *et al*. [30] has successfully produced overstorey 1-km LAI by incorporating one-degree MISR background reflectance to the UofT v1 LAI algorithm for GLOBCARBON product. Based on [30], our aim here is to account for the topographical effects in the removal of the background contribution from the pixel-level SR through considering the solar and view incidence angles to sloping surfaces. Therefore, the new SR to be used for LAI inversion in (5) and (6) based on incidence view-target-sun angles is as follows:

$$SR = SR_{pixel} + (2.4 - SR_b) \cos\gamma_s \frac{(SR_{max} - SR_{pixel})\cos\gamma_v}{(SR_{max} - SR_b)} \quad (7)$$

where SR_{pixel} is the original measured (understorey + overstorey) value from MODIS data, SR_{max} is the maximum SR value for a specific view-sun incidence angle combination and cover types, SR = 2.4 is a standard soil background values used in model simulations and in the UofT v1 LAI product. The term $[(SR_{max} - SR_{pixel})/(SR_{max} - SR_b)]$ is a gap fraction. Unlike [30], the bi-directional gap fraction effect is considered here in both viewing and illumination incidence directions. Both the new view and sun incidence angles computed from slope and aspect of the pixel for LAI and background computation were first approximated to the ranges provided by [10] to keep the internal consistency of the entire workflow. Although the background types and reflectances are usually similar over wide geographic region [31], small uncertainties related with the spatial resolution of the input background SR for 250-m LAI product will remain. However, the input background varies monthly, which is assumed to address the seasonal trajectory of background brightness variations in order to produce canopy LAI product.

4) Foliage Element Clumping Index Data: Previous products of the UofT v1 LAI algorithm, such as GLOBCARBON LAI were based on an empirical clumping index (Ω) fixed per land cover type as provided in [32]. Pisek *et al*. [30] in a later study has applied the spatially explicit clumping index derived from POLDER-3 data at 6-km spatial resolution. However, this product is too coarse for our 250-m LAI algorithm. Therefore, in this paper in order to generate the UofT v2 LAI product, we have used the spatially explicit clumping index derived from the MODIS BRDF/Albedo products at 500-m resolution. Ω is sensitive to plant canopy architecture by that to plant functional types; therefore, it is expected

to be less sensitive within the four pixels of 250-m LAI product contained for every 500-m pixel of Ω product. The Ω computation follows the same approach as [32], which was based on normalized difference between hotspot and darkspot (NDHD) index. However, for the current study, the hotspot and darkspot information were derived from the red band of MODIS MCD43 500-m v005 BRDF parameters retrieved using RossThick-LiSparse reciprocal BRDF model [33]. The new MODIS-based global Ω product is currently undergoing large validation exercises [34]. Details of the processing and performance assessments of the 500-m global Ω product are given in [34]. The global validation exercise results in an estimated and measured Ω correlation coefficient of determination of 76% and a root mean square error (RMSE) of 0.12, theretofore ascertaining confidence to use for operational estimation of LAI values.

D. LAI Intercomparison Approach

One of the first steps for the evaluation of the 250-m MODIS-based UofT LAI products for both v1 (not corrected for pixel-by-pixel topography, background reflectance, and clumping index) and v2 was to compare with measured data. It is important that the MODIS-based UofT v1 product to be evaluated as well since it consists a new input data and processing scheme (Fig. 1) compared to the previously used SPOT VGT data. Two direct and indirect validations are conducted: 1) evaluation of the LAI estimates on flat ground based on *in situ* measurements over fluxnet sites before temporal smoothing of the UofT LAI estimates and 2) evaluation of the UofT LAI estimates on sloping ground using MODIS and reference LAI map after temporal smoothing.

1) In Situ Measurements in Canadian Carbon Program (CCP) Fluxnet Sites: We have used all available ensembles of LAI measurements collected by LAI-2000 plant canopy analyzer and TRAC instruments over CCP fluxnet forest sites, measured in growing seasons of 2003–2005 [35]. The description for all 17 CCP fluxnet tower sites is given in [35] and [36]. The tower sites are mostly large homogeneous forest stands (>1 km^2). The LAI data from these tower flux sites are therefore appropriate for validating our new LAI product at 250-m resolution without spatial scaling using high resolution remote sensing images [37], [38]. The 10-day MODIS data composites used here for comparison with ground measurements are from June 21–30, July 1–10, and July 11–20, 2005. After deriving LAI using both UofT v1 and v2 LAI algorithms from the three datasets at 250 m, we extracted the median values to compare with the ground measurements in order to avoid any remnant cloud and cloud-shadow effects on LAI estimations.

LAI-2000 measurements were conducted in 14 whereas TRAC measurements in 15 CCP fluxnet sites. At each site, LAI measurements were made along one or two transects of length ranging from 60 to 400 m depending on the homogeneity and size of a site following LAI measurement protocol given in [37] to estimate all needed parameters, such as effective LAI, needle-to-shoot area ratio, woody-to-total area ratio, and clumping index. This is based on labor intensive
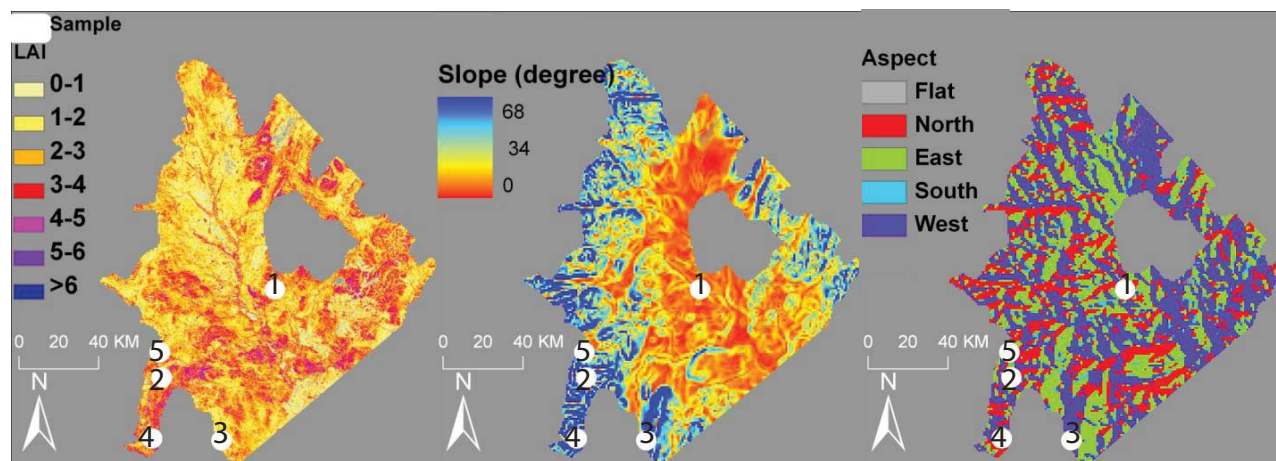
Fig. 2. LAI distribution in Watson Lake area displayed with terrain slope and aspect of the study area. The numbered white dots indicate the 3 by 3 km sample points for LAI intercomparison representing various land cover, terrain slope, and aspect of the pixel orientations. The characteristics of the five sampling points identified by their numbers are given in Table I.

field campaign to obtain each of the necessary parameters; however; in the cases of missing measurements for needle-to-shoot and woody-to-total area ratio parameters, forest type and age specific values were used based on previous surveys [35], [39]–[41].

The effective LAI obtained from both TRAC and LAI-2000 were used as independent evaluation measures for the UofT effective LAI estimates. The LAI corrected for clumping index was instead obtained based on: 1) TRAC LAI from TRAC effective LAI and TRAC clumping index measures and 2) LAI-2000 + TRAC LAI from LAI-2000 effective LAI and TRAC clumping index measures. The corresponding LAI and effective LAI estimates from U of Tv1 and v2 LAI algorithms were extracted from a single 250-m pixel overlapping the ground measurement transects.

2) Comparison With Reference LAI Map and MODIS Collection 5 LAI Product: Reference LAI map we have used a high-resolution (30 m) LAI map produced over Watson Lake area, Yukon Territory, Canada for July, 2000 [42]. This area, located close to the border of British Columbia and Yukon, corresponds to approximately 17 000 km² centered at 60.10 N and 129.69 W (Fig. 2). The area is dominated by boreal forests of white spruce, black spruce, lodgepole pine, and trembling aspen growing on mostly sloping ground. The understory and open areas are characterized by alpine tundra communities of lichens, dwarf ericaceous shrubs, birch, and willows (available at: http://www.ec.gc.ca/soerree/English/ Framework/ default.cfm). The area is characterized by slow growing conifer stands, as a result only seasonal LAI variations are assumed to be conspicuous. The map was obtained from the distributed active archive center (DAAC) database of Oak Ridge National Laboratory (available at: http:// daac.ornl.gov / VEGETATION / guides / Fernandes_LAI.html). The map was produced by upscaling a set of *in situ* optically based LAI estimates collected using at least ten points of LAI-2000 measurements and two 50-m TRAC transects per plot over 18 plots of approximately 1ha each within

the mapped area. Plots were located on flat ground using a land cover-based stratified random sampling technique. The retrieved LAI is a true canopy LAI value corrected for foliage element clumping excluding understorey vegetation below the *in situ* instrument sensors. The infrared simple ratio (ISR) derived from NIR and SWIR bands of Landsat ETM+ data corrected for atmospheric effect using 6S model were used as an upscaling variable in the transfer function. The transfer function is based on the LAI versus ISR relationship derived using the Thiel–Sen regression approach [12], [43]. No corrections for topography and slope were made for the ETM+ image.

MODIS LAI product: MODISTerra Collection 5 (MOD15A2) 1-km LAI product was acquired as ASCII subsets over selected sample sites of Watson Lake area from the DAAC database of Oak Ridge National Laboratory (available at: http://daac.ornl.gov/MODIS/). We acquired LAI values for five sites of 3 by 3 km using a JAVA client from the MODIS web service, which is built on ORNL DAACs MODIS Global subsetting and visualization tool providing customized subsets and visualization of MODIS land products for any land location on the globe. The acquired MODIS Collection 5 LAI product is composited every eight days using a main retrieval algorithm based on a 3-D radiative transfer model tuned for eight main biome classes [44]. The MODIS LAI is retrieved from LUTs generated using a stochastic 3-D radiative transfer model over a satellite pixel radiative transfer field. The simulation of 3-D effects of vegetation heterogeneity (foliage clumping and species mixture) is based on observed and modeled red and NIR bi-directional reflectance factor (BRF) for a combination of canopy structures, leaf optical properties, and soil/background patterns that represent an expected range of typical conditions for a given biome type [45]. Each pixel can have a background ranging from dark soil to bright soils. The algorithm compares the observed and modeled BRFs and the mean LAI value is taken over all acceptable solutions obtained from a suite of canopy structures, leaf optical properties, and soil/background

TABLE I

FIVE SELECTED 3 BY 3 km SAMPLE SITES IN WATSON LAKE AREA FOR LAI INTERCOMPARISON

Sample	Lat.	Long.	Slope	Aspect	Land Cover (UofT)	Land Cover (MODIS)	Reference LAI (year 2000)
1	60.030	−129.130	0	Flat	Needleleaf forest	Needleleaf forest	3.34
2	59.407	−129.602	10	East	Mixed forest and shrub	Needleleaf forest, shrub and grass	2.87
3	59.297	−128.842	12	West	Mixed forest, shrub and grass	Needleleaf forest, shrub and grass	2.55
4	59.141	−129.391	17	South	Mixed forest, shrub and grass	Needleleaf forestand shrub	2.86
5	59.503	−129.738	9	North	Mixed forest and shrub	Needleleaf forestand grass	2.41

patterns. As such, MODIS LAI production scheme uses theoretical values expected for each biome rather than a measured background and clumping index values. Snow and understorey background reflectivities are not considered in the assumed theoretical background radiative transfer fields of the pixel. The MODIS LAI represents a true LAI corrected for clumping and background reflectances, although the implementation and the physical properties of both clumping and background reflectivity differ significantly with that of the UofT LAI algorithm. This is expected to be one of the major causes of differences between UofT and MODIS LAI products. No topographic consideration is employed in the MODIS algorithm.

The UofT v1 and v2 LAI results were compared with the reference LAI map and MODIS LAI product. The Watson Lake reference LAI map is derived for July, 2000. The UofT LAI used for the comparison are from the reference year 2008, which is chosen for forest carbon studies in Canada and proximity to background and clumping index measurements. To account for the large temporal gaps between the reference LAI map (year 2000) and the UofT LAI product (year 2008), we use MODIS 2000 and 2008 time series as a reference for interannual variation of LAI over the selected sites of Watson Lake area. The comparison of LAI time series for the five selected sites over Watson Lake area from the two MODIS measurements, i.e., year 2000 and 2008, confirms that the interannual variation of LAI is negligible. This gives us confidence to validate the UofT LAI product from year 2008 using a reference LAI map from year 2000 measurements. Five sites of 3 by 3 km were selected to represent various land cover, terrain slope, and aspect (Table I, Fig. 2). The selection is based on uniform terrain aspect of pixels within a 3 by 3 km area.

III. RESULTS AND DISCUSSION

A. Comparison With In Situ LAI Measurements

Fig. 3 compares 250-m effective LAI estimates from UofT v1 and v2 LAI algorithms with the ground measurements in CCP fluxnet forest sites. All of the relationships between estimates and measurements presented in Fig. 3 are statistically significant at p-value of 0.05, indicating that the estimates explain the measured LAI variations. The mean ground measurement of effective LAI from LAI-2000 and TRAC for the common ground plots were 3.7 and 3.9, respectively, whereas 4.2 and 5.8 were obtained from UofT v2 and v1 LAI algorithms, respectively. The main reason for higher estimates
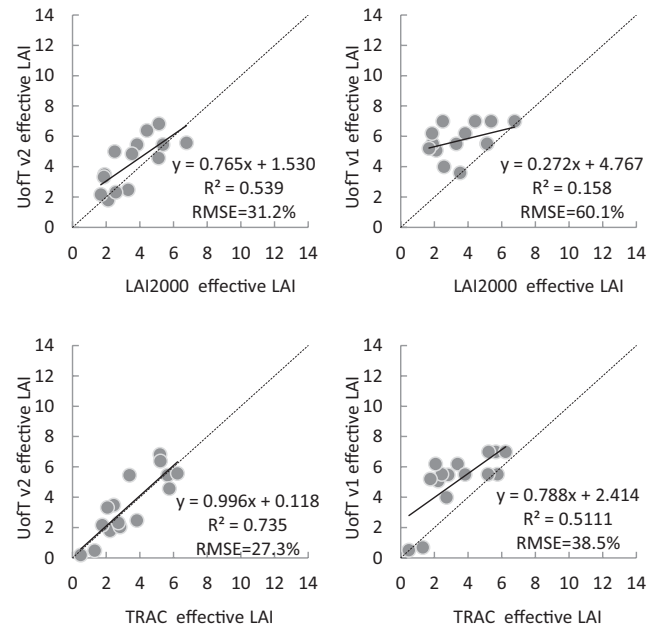

Fig. 3.   Comparison between the *in-situ* canopy effective leaf area index (LAI) values to the corresponding canopy effective LAI estimates from UofT v1and v2 LAI algorithms. Scatter plots are provided for the CCP fluxnet forest sites [35]. The solid diagonals correspond to regression lines and the dashed diagonals are the 1:1 lines. RMAE: relative median absolute error.

of effective LAI from v1 compared to v2 is that in v1 the background reflectance is fixed to the comparably low standard soil SR value (SR = 2.4) used in the model whereas, in v2 and for the ground measurements, the estimates represent the actual canopy effective LAI. The effect of slope correction in v2 is negligible because all of the ground measurements are collected from flat ground of CCP fluxnet tower sites. Therefore, the effective LAI estimates from the UofT v2 LAI algorithm show regression slope close to unity and comparable mean LAI estimates with the ground measurements (Fig. 3). The relative median absolute error (RMAE) obtained from the UofTv1 (v2) LAI algorithms of effective LAI estimates compared with LAI-2000 and TRAC measurements are 60% (31%) and 39% (27%), respectively. The overall results indicate significant improvement in v2 compared to UofT v1LAI estimates for effective LAI estimates.

The LAI corrected for clumping index based on pixel-by-pixel value in v2 and empirically determined land cover-specific value in v1 have resulted in less correlation compared to the corresponding effective LAI results (Fig. 4). However, all of the relationships between estimates and measurements
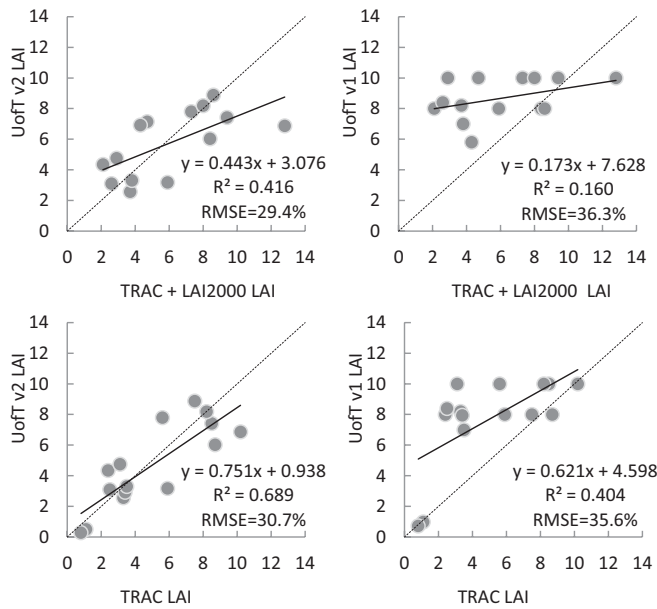
Fig. 4. Comparison between the *in-situ* canopy LAI values to the corresponding canopy LAI estimates from UofT v1and v2 LAI algorithms. Scatter plots are provided for the CCP fluxnet forest sites [35]. The solid diagonals correspond to regression lines and the dashed diagonals are the 1:1 lines. RMAE: relative median absolute error.
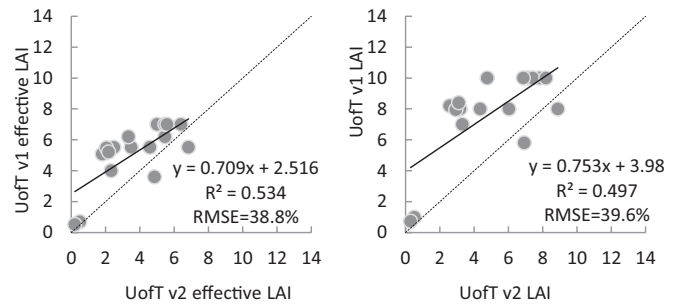

Fig. 5. Comparison between the corresponding canopy effective LAI and LAI values estimates from UofT v1 and v2 LAI algorithms. Scatter plots are provided for the CCP fluxnet forest sites [35]. The solid diagonals correspond to regression lines and the dashed diagonals are the 1:1 lines. The upper end LAI (effective LAI) values for saturated pixels are 10 (7), and 8 (5) for needleleaf or deciduous forests, and sub-polar taiga needleleaf or mixed forests, respectively. RMAE: relative median absolute error.

presented in Fig. 4 are statistically significant at *p*-value of 0.05, indicating that the estimates explain the measured LAI variations. The mean ground measurement of LAI from LAI-2000 +TRAC and TRAC for the common ground plots were 6.3 and 5.8, respectively, whereas 5.5 and 8.8 where obtained from UofT v2 and v1 LAI algorithms, respectively. The RMAE obtained from UofT v1 (v2) LAI algorithms of LAI estimates compared with LAI-2000 +TRAC and TRAC measurements were 36% (29%) and 35.6% (30.7%), respectively. The effect of the effective LAI saturation due to a background reflectance misrepresentation in v1 is also conspicuous in the clumping corrected LAI estimates. As for v2 comparison with ground measurements, the main discrepancy compared to the performance of effective LAI comes from the difference of clumping index between ground measurements and MODIS BRDF products. In both Figs. 3 and 4, one can notice the effect of variations in clumping index used among the ground measurements (mean = 0.93), land cover-specific values in UofT v1 LAI algorithm (mean = 0.7), and pixel-by-pixel estimates in UofT v2 LAI algorithm (mean = 0.65) on the performance differences obtained between LAI and effective LAI. The performance of the pixel-based clumping index used in UofT v2 LAI algorithm is given in [33]. Overall, the variation of LAI estimates among the ground measurements, UofT v1 and v2 LAI algorithms, merely due to the differences in clumping index, is below 7%. The overall performance assessments, such as the slope, intercept of regression line, mean estimated values, and the RMAE indicate that the v2 has resulted in improved LAI estimates compared to UofT v1 LAI algorithm.

There can be several reasons for why there are still modest results from UofT v2 LAI algorithm compared to ground measurements. One of the sources of errors can be from the ground measurements as summarized in [35] for the *in situ* data used in this paper. These errors could be from saturation of measurable gaps as most of the CCP fluxnet sites are characterized by dense forest. At high LAI, optical *in situ* instruments are known to perform poorly [19], [35], [46]. We have used the best available ground estimates compiled from the 2003–2005 growing seasons. Aside from the temporal difference in LAI estimates, the total error of ground measurements could be in range of 35% for the CCP fluxnet forest sites: 10% error coming from woody-to-total area ratio, 5% error in effective LAI, 5% in needle-to-shoot error ratio, and 5% in element clumping index above shoot level and upto 10% error from very dense tree crowns, such as the black spruce stands of CCP fluxnet sites [19], [35], [39].

Sources of errors for UofTv1 and v2 LAI estimates can still be found in the time difference with ground measurements, remnant cloud contamination, geo-location mismatch with ground plots, coarse resolution inputs for background reflectances, and clumping index for v2 and land cover-specific values in v1. It is apparent that the background reflectance highly influences the performance of the LAI algorithms. In some CCP fluxnet sites, the actual background LAI can be as large as the canopy LAI [35]. This effect of background reference is however captured in v2 algorithm although there can still be significant error as the background has coarser resolution compared to the reflectance measurements and the LAI product. Considering the often modest performances of regional LAI products [13], [21], the results obtained in this paper have shown acceptable performance. The effects from the direct scaling of ground measurement to satellite pixel are assumed to be minimal in this paper as most of the forest sites were homogeneous and the plot transects were large enough to cover at least one pixel. Fig. 5 presents the comparison of canopy effective LAI and LAI as estimated using UofT v1 and v2 LAI algorithms for the CCP fluxnet sites presented in Figs. 3 and 4. The result indicates that effective LAI up to 4 and LAI up to 6 were comparable from the two UofT LAI algorithm versions. For larger LAI and effective LAI, v1 has overestimated LAI compared to UofT v2 LAI algorithm (Fig. 5) and ground measurements (Figs. 3 and 4).
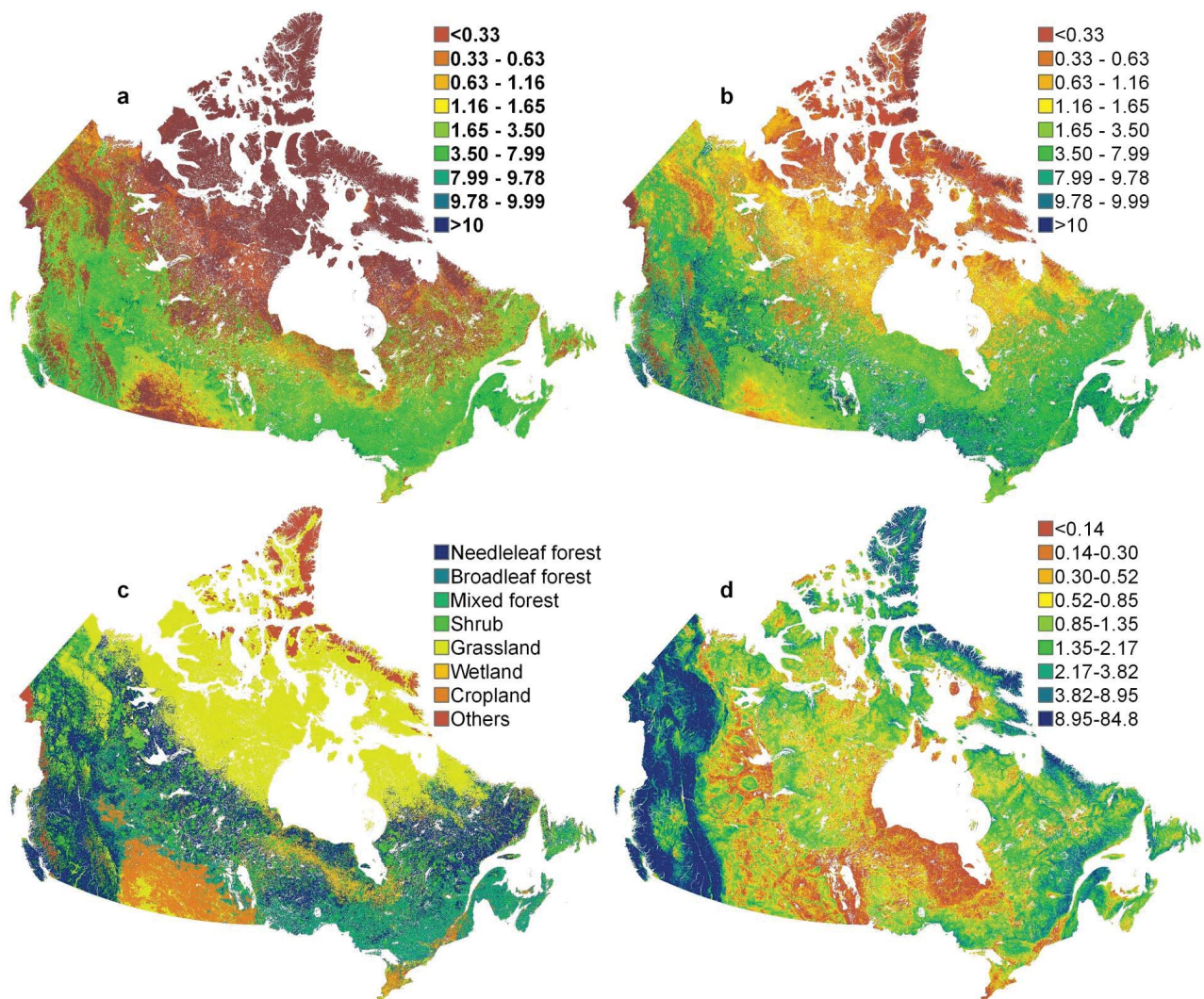
Fig. 6. 250-m map of LAI distribution over Canada. (a) LAI from UofT v2 LAI algorithm. (b) LAI from UofT v1 LAI algorithm. (c) 500-m land cover map derived from MODIS data. (d) Slope angle in degrees.

This indicates that UofT LAI algorithm has been significantly improved.

B. Spatial Characteristics

Fig. 6(c) shows the land cover distribution over Canada for qualitative evaluation of the LAI maps. LAI is expected to be higher in forested regions and lower in nonforest vegetations whereas geographically the southern vegetated land covers have higher LAI than the corresponding land covers in northern latitudes. One also expects higher LAI in needleleaf forests followed by mixed forest and broadleaf forest. Among the needleleaf forest, the western temperate forests exhibit larger LAI compared to other boreal needleleaf forests due to the geophysical and climatological factors. These patterns are fully captured in the UofT LAI products [Fig. 6(a) and (b)]. This however does not imply that the same reflectance values in various land cover equal the same LAI. As part of the development of the UofT v2 LAI algorithm, we have extensively analyzed the land cover impacts on LAI estimation [28].

Both v1 and v2 explain the variability of LAI compared to the land cover map presented in Fig. 6–high LAI values over forest vegetation, intermediate LAI over crop and wetlands, and low LAI over northern shrub and grass lands. 79% of estimates from both versions resulted in less than a unity, with LAI differences in absolute value with closely resembling distributions. Whereas, 19% of land pixels resulted in zero difference of estimated LAI mainly corresponding to the saturated pixels in both versions [Fig. 6(a) and (b)]. The major difference at around LAI value of eight and ten, which are the upper end saturation values for shrub or grass, and forest land covers, respectively, is due to the relatively low background fixed SR (2.4) value used in v1. This is in accordance with the results presented in Section III-A. with ground measurement comparisons. The other disparities both in forest and nonforest vegetated land cover types come from the interrelated effects of background, clumping, and slope consideration differences in both versions. Fig. 6(a) and (b) shows that the major difference in estimated LAI is in forest transition zones except in the Rocky Mountains of Western Canada where the differences
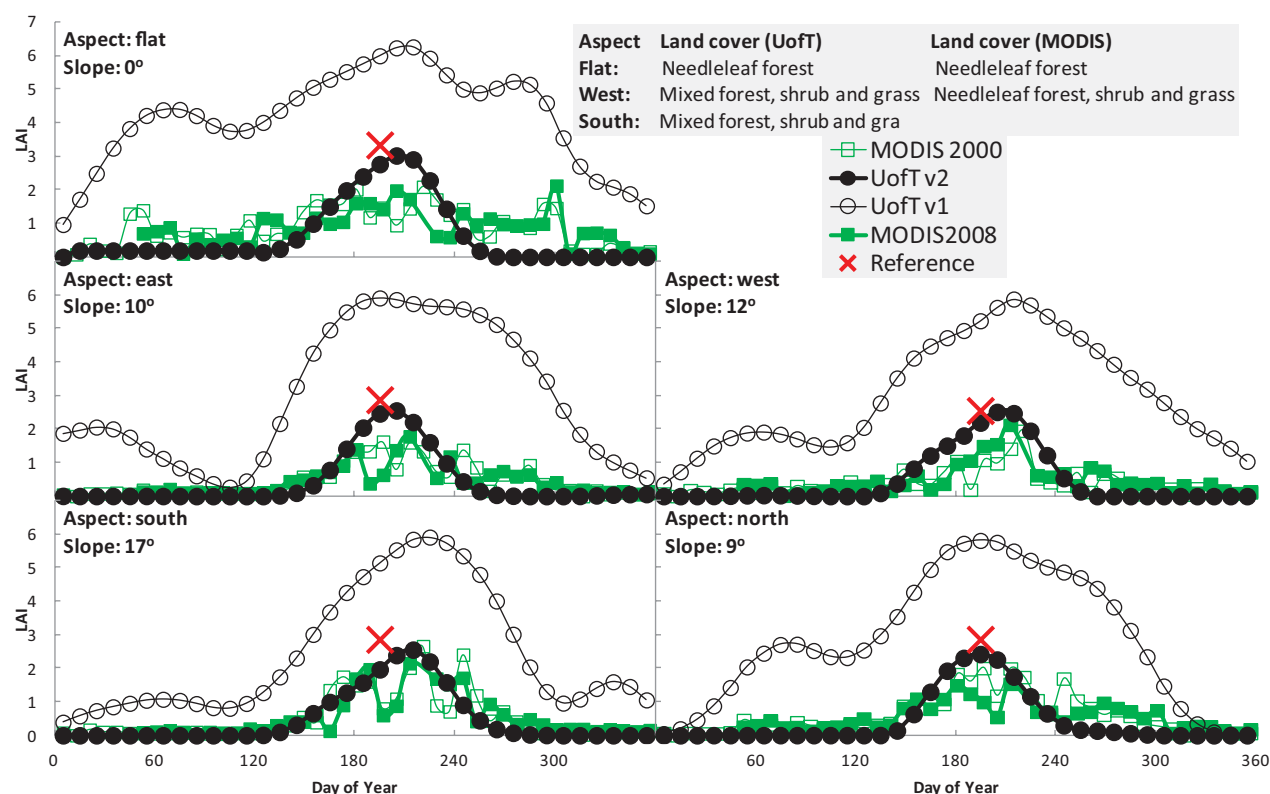
Fig. 7. Temporal evolution of UofT v1 and v2 LAI 2008 product plotted along with MODIS 2000 and 2008 LAI product and reference LAI map from year 2000 over sloping terrain of 3 by 3 km sample sites. The five sites characteristics are given in Table I. The interannual similarity of LAI estimates between the year 2000 and 2008 from MODIS product confirms that the five selected intercomparison sites are stable in LAI magnitude. These sites show only seasonal variations. The MODIS LAI products from year 2000 and 2008 give a control for the evaluation of UofT LAI products for year 2008 using the ground LAI reference value from year 2000.

are over the entire forest landscape. This indicates that slope has a large effect on the estimated LAI.

C. Comparison With Reference LAI Map and MODIS LAI Product

The temporal evolution of LAI estimates from UofT and MODIS products over sloping ground is shown in Fig. 7. The interannual similarity of LAI estimates between the year 2000 and 2008 from MODIS product confirms that the five selected intercomparison sites are stable only showing seasonal variations. The seasonal LAI variations of all products have shown expected trends with UofT v1 LAI algorithm overestimating and MODIS product underestimating the LAI compared to the reference map and UofT v2 LAI algorithm. Neither the MODIS nor the reference LAI maps are corrected for slope. However, the results of the flat site giving consistent trend as the sloping grounds assures us that overall the UofT v2 LAI algorithm performs best. The LAI estimates from UofT v2 LAI algorithm resulted in the closest estimates as compared to the reference LAI map with maximum LAI values ranging between 2.5 and 3, comparable to the reference map (Table I) and variations within 0.5 LAI units compared to the reference map. Despite the fact that MODIS LAI product went through several validations, to the best of our knowledge none of the studies were conducted on sloping ground.

Table I gives the land cover types used to retrieve the MODIS and UofT LAI values for the selected sample sites.

The land cover types are similar for most of the pixels selected in the sampling sites. However, there can still be significant LAI variation due to land cover differences between UofT and MODIS LAI estimates. We have previously evaluated the effect of land cover on UofT LAI algorithm as a part of developing the UofT v2 LAI algorithm [28]. The pixel-by-pixel mean absolute difference of 0.665 (42%) LAI obtained using the improved UofT v2 LAI algorithm over Canada based on the GLC2000 and NALC2005 land cover datasets shows that land cover misclassification is a great source of uncertainty for LAI estimation [28]. Although there are no comparable studies for the effect of land cover on MODIS LAI retrieval, [47] calculated the LAI difference to be up to 244% when distinct biomes are misclassified for a given pixel in the global MODIS LAI product, the sever effect occurring between the needleleaf and grass/crop misclassification. The assumption that vegetation within each pixel belongs to one of the major biomes impacts the LAI retrievals. This is however expected to be minimal in the UofT v2 LAI algorithm due to the use of improved land cover product (NALC2005) with higher pixel spatial resolution (250 m) compared to MODIS land cover used in LAI retrieval [28].

We have conducted further sensitivity analysis to evaluate the relative contribution of each improvement in UofT v2 compared to UofT v1 product (not shown here for brevity). The results indicated that the main difference between v1 and v2 LAI estimates is due to the background reflectance

correction. Originally, the UofT LAI algorithm was designed to incorporate background reflectance. This was, however, not possible at the time of v1 global LAI product for GLOB-CARBON project due to the lack of multiangular information. At the time, this did not represent a serious problem for closed canopy forests. With the advent of Earth observation systems featuring multiangular capabilities, an update of the UofT LAI algorithm became possible enabling the removal of background reflectances. As the MODIS reflectance measurements are acquired in one direction, portioning the vertical profile into understory and overstorey is currently not possible. The terrain effect cannot solely be traced in Fig. 7 due to the interrelated improvements implemented in UofT v2 LAI algorithm, for instance, the relative contribution of background reflectance depends on the slope and aspect of the pixel (7). Due to lack of ground measurements on sloping ground, the slope correction needs further evaluation. LAI estimation over sloping ground even for the *in situ* reference instruments is challenging [22].

IV. CONCLUSION

The improvement of UofT LAI algorithm based on MODIS reflectance data at 250-m resolution was demonstrated using ground LAI measurements from 17 forest stand flux tower sites across Canada. The MODIS-based land cover map at the same spatial resolution was used for LAI retrieval. The improvement was achieved through pixel-by-pixel consideration of local topography, clumping index, and background reflectance variations. The differences of the LAI derived using UofT v2 and v1 LAI algorithms were found to be the largest in mountainous areas in British Columbia province, as the v1 algorithm does not consider the topographic effect. This suggested that topographic effect needs further attention for improvement of LAI algorithms. Ground LAI measurements in mountainous areas are challenging and scarce. As the regional and global remote sensing capabilities improve in terms of spatial resolution, the need of detailed consideration of topographic effect becomes apparent. In the future, we aim to produce the global UofT v2 LAI time series product using the standard MODIS reflectance products based on seasonally variable MODIS-based clumping index, background reflectance, and local topography. The improved product will be used as an enhanced spatial variable for Integrated Terrestrial Ecosystem Carbon model (InTEC) [48], boreal ecosystem productivity simulator (BEPS) [49], and CBM-CFS models for carbon budget studies on Canadian landmass and eventually on the global scale.

The large overestimation of v1 LAI estimate compared to the ground measurements was explained by the overestimation of the effective LAI mainly due to underestimation of background reflectance contribution to canopy reflectance in v1 algorithm. However, both LAI and effective LAI from TRAC were significantly correlated with UofT v2 LAI algorithm values. The evaluations of UofT v1 and v2 LAI estimates were carried out using the carefully acquired ground measurements [35]. The results were expected to improve in further progress of UofT v2 LAI algorithm when high resolution

~250–500-m background reflectance derived from MODIS BRDF/Albedo parameters or from any upcoming multiangular sensors were incorporated. We also aimed to produce seasonal clumping index estimates at the same spatial resolution in future studies. Other overlooked bias in ground measurements comes from the overestimation of measured clumping index (underestimation of foliage element clumping) as the TRAC instrument is walked under forest canopy where small gaps are hardly visible. The ground estimates of clumping index and its relation with canopy height and height of measurement need careful attention. The UofT v2 LAI algorithm was developed in order to produce a new generation of regional and eventually global 250-m LAI time series products.

Generally speaking, the main difference of LAI estimates between UofT v1 and v2 algorithms is due to the background reflectance consideration followed by pixel-by-pixel clumping index and last slope corrections. The indirect comparison with a MODIS LAI product and a reference LAI map on sloping ground has revealed that the UofT v2 LAI algorithm showed significant improvement compared to the previous version. However, this does not imply either MODIS or reference LAI maps on sloping ground represent the absolute reference. MODIS considers BRF in contrast to the LAI-BRDF relationships used in UofT LAI algorithms. Although, the BRF is less sensitive for sloping ground, the bias introduced by assuming all vegetation surfaces as lambertian reflectors in the MODIS product introduces errors related with view-target-sun geometry variation effects on measured reflectances.

This paper further emphasizes that land remote sensing particularly for vegetated surfaces needs special attention for terrain effects. Most of the satellite land product validation studies have so far been conducted in temperate regions or on flat and homogeneous sites where topography is usually not the main concern. However, globally, a significant amount of forest grows on hilly terrain and on steep slopes. This entails to validate remote sensing-based land surface products on sloping ground and complex terrains. Future validation activities also should consider producing LAI reference measurements and maps, which are compensated for topographic effects.

REFERENCES

[1] W. A. Kurz, C. C. Dymond, T. M. White, G. Stinson, C. H. Shaw, G. J. Rampley, C. Smyth, B. N. Simpson, E. T. Neilson, J. A. Trofymow, J. Metsaranta, and M. J. Apps, "CBM-CFS3: A model of carbon-dynamics in forestry and land-use change implementing IPCC standards," *Ecol. Model.*, vol. 220, no. 4, pp. 480–504, Feb. 2009.
[2] A. D. McGuire, S. Sitch, J. S. Clein, R. Dargaville, G. Esser, J. Foley, M. Heimann, F. Joos, J. Kaplan, D. W. Kicklighter, R. A. Meier, J. M. Melillo, B. Moore, I. C. Prentice, N. Ramankutty, T. Reichenau, A. Schloss, H. Tian, L. J. Williams, and U. Wittenberg, "Carbon balance of the terrestrial biosphere in the twentieth century: Analyses of CO_2, climate and land use effects with four process-based ecosystem models," *Global Biogeochem. Cycles*, vol. 15, no. 1, pp. 183–206, Mar. 2001.

[3] A. P. Trishchenko, "Concept of a new multiangular satellite mission for improved bidirectional sampling of surface and atmosphere properties," *Proc. SPIE*, vol. 5542, pp. 97–108, Nov. 2004.

[4] *Implementation Plan for the Global Observing System for Climate in Support of the UNFCCC*, GCOS Standard GCOS-92, 2004.

[5] J. M. Chen and T. A. Black, "Defining leaf-area index for non-flat leaves," *Plant Cell Environ.*, vol. 15, no. 4, pp. 421–429, May 1992.

[6] A. Gonsamo, "Remote sensing of leaf area index: Enhanced retrieval from close-range and remotely sensed optical observations," Ph.D. dissertation, Dept. Geography, Univ. Helsinki, Helsinki, Finland, Dec. 2009.

[7] S. O. Los, G. J. Collatz, P. J. Sellers, C. M. Malmström, N. H. Pollack, R. S. DeFries, L. Bounoua, M. T. Parris, C. J. Tucker, and D. A. Dazlich, "A global 9-yr biophysical land surface dataset from NOAA AVHRR data," *J. Hydromet.*, vol. 1, no. 2, pp. 183–199, Apr. 2000.

[8] V. Masson, J. L. Champeaux, F. Chauvin, C. Meriguet, and R. Lacaze, "A global database of land surface parameters at 1-km resolution in meteorological and climate models," *J. Clim.*, vol. 16, no. 9, pp. 1261–1282, May 2003.

[9] F. Baret, O. Hagolle, B. Geiger, P. Bicheron, B. Miras, M. Huc, B. Berthelot, F. Nino, M. Weiss, O. Samain, J. L. Roujean, and M. Leroy, "LAI, fAPAR and fCover CYCLOPES global products derived from VEGETATION-part 1: Principles of the algorithm," *Remote Sens. Environ.*, vol. 110, no. 3, pp. 275–286, Oct. 2007.

[10] F. Deng, J. M. Chen, S. Plummer, and J. Pisek, "Algorithm for global leaf area index retrieval using satellite imagery," *IEEE Trans. Geosci. Remote Sens.*, vol. 44, no. 8, pp. 2219–2229, Aug. 2006.

[11] W. Yang, N. V. Shabanov, D. Huang, W. Wang, R. Dickinson, R. Nemani, Y. Knyazikhin, and R. Myneni, "Analysis of leaf area index products from combination of MODIS Terra and Aqua data," *Remote Sens. Environ.*, vol. 104, no. 3, pp. 297–312, Oct. 2006.

[12] R. Fernandes, C. Butson, S. Leblanc, and R. Latifovic, "Landsat-5 TM and Landsat-7 ETM$^+$ based accuracy assessment of leaf area index products for Canada derived from SPOT-4 VEGETATION data," *Can. J. Remote Sens.*, vol. 29, no. 2, pp. 241–258, Apr. 2003.

[13] S. Garrigues, R. Lacaze, F. Baret, J. T. Morisette, M. Weiss, J. E. Nickeson, R. Fernandes, S. Plummer, N. V. Shabanov, R. B. Myneni, Y. Knyazikhin, and W. Yang, "Validation and intercomparison of global-leaf area index products derived from remote sensing data," *J. Geophys. Res., Biogeosci.*, vol. 113, no. G2, pp. 1–20, Jun. 2008.

[14] F. Canisius, R. Fernandes, and J. Chen, "Comparison and evaluation of medium resolution imaging spectrometer leaf area index products across a range of land use," *Remote Sens. Environ.*, vol. 114, no. 5, pp. 950–960, May 2010.

[15] J. M. Chen and S. G. Leblanc, "A four-scale bidirectional reflectance model based on canopy architecture," *IEEE Trans. Geosci. Remote Sens.*, vol. 35, no. 5, pp. 1316–1337, Sep. 1997.

[16] J. M. Chen and S. G. Leblanc, "Multiple-scattering scheme useful for geometric optical modeling," *IEEE Trans. Geosci. Remote Sens.*, vol. 39, no. 5, pp. 1061–1071, May 2001.

[17] J.-L. Roujean, M. Leroy, and P.-Y. Deschamps, "A bidirectional reflectance model of the Earth's surface for the correction of remote sensing data," *J. Geophys. Res., Atmos.*, vol. 97, no. D18, pp. 20455–20468, Jan. 1992.

[18] J. M. Chen and J. Cihlar, "A hotspot function in a simple bidirectional reflectance model for satellite applications," *J. Geophys. Res., Atmos.*, vol. 102, no. D22, pp. 25907–25913, Dec. 1997.

[19] J. M. Chen, P. M. Rich, S. T. Gower, J. M. Norman, and S. Plummer, "Leaf area index of boreal forests: Theory, techniques, and measurements," *J. Geophys. Res. D, Atmos.*, vol. 102, no. D24, pp. 29429–29443, Dec. 1997.

[20] J. M. Chen, F. Deng, and M. Chen, "Locally adjusted cubic-spline capping for reconstructing seasonal trajectories of a satellite-derived surface parameter," *IEEE Trans. Geosci. Remote Sens.*, vol. 44, no. 8, pp. 2230–2238, Aug. 2006.

[21] J. Pisek, J. M. Chen, and F. Deng, "Assessment of a global leaf area index product from SPOT-4 VEGETATION data over selected sites in Canada," *Can. J. Remote Sens.*, vol. 33, no. 4, pp. 341–356, Aug. 2007.

[22] A. Gonsamo and P. Pellikka, "Methodology comparison for slope correction in canopy leaf area index estimation using hemispherical photography," *Forest Ecol. Manag.*, vol. 256, no. 4, pp. 749–759, Aug. 2008.

[23] A. Gonsamo and P. Pellikka, "The computation of foliage clumping index using hemispherical photography," *Agric. For. Meteorol.*, vol. 149, no. 10, pp. 1781–1787, Oct. 2009.

[24] A. P. Trishchenko, Y. Luo, and K. V. Khlopenkov, "A method for downscaling MODIS land channels to 250-m spatial resolution using adaptive regression and normalization," *Proc. SPIE*, vol. 6366, p. 636607, Oct. 2006.

[25] Y. Luo, A. P. Trishchenko, and K. V. Khlopenkov, "Developing clear-sky, cloud and cloud shadow mask for producing clear-sky composites at 250-meter spatial resolution for the seven MODIS land bands over Canada and North America," *Remote Sens. Environ.*, vol. 112, no. 12, pp. 4167–4185, Dec. 2008.

[26] A. Gonsamo and J. M. Chen, "Spectral response cross-calibration among 21 satellite sensors for vegetation monitoring," *IEEE Trans. Geosci. Remote Sens.*, vol. 51, no. 3, pp. 1319–1335, Mar. 2013.

[27] E. F. Vermote, D. Tanre, J. L. Deuze, M. Herman, and J. J. Morcette, "Second simulation of the satellite signal in the solar spectrum, 6S: An overview," *IEEE Trans. Geosci. Remote Sens.*, vol. 35, no. 3, pp. 675–686, May 1997.

[28] A. Gonsamo and J. M. Chen, "Evaluation of GLC2000 and NALC2005 land cover products for LAI retrieval over Canada," *Can. J. Remote Sens.*, vol. 37, no. 3, pp. 302–313, Jun. 2011.

[29] J. Pisek and J. M. Chen, "Mapping forest background reflectivity over North America with multi-angle imaging spectroradiometer (MISR) data," *Remote Sens. Environ.*, vol. 113, no. 11, pp. 2412–2423, Nov. 2009.

[30] J. Pisek, J. M. Chen, K. Alikas, and F. Deng, "Impacts of including forest understory brightness and foliage clumping information from multiangular measurements on leaf area index mapping over North America," *J. Geophys. Res. Biogeosci.*, vol. 115, no. G3, p. G03023, Sep. 2010.

[31] S. P. Serbin, S. T. Gower, and D. E. Ahl, "Canopy dynamics and phenology of a boreal black spruce wildfire chronosequence," *Agric. For. Meteorol.*, vol. 149, no. 1, pp. 187–204, Jan. 2009.

[32] J. M. Chen, C. H. Menges, and S. G. Leblanc, "Global mapping of foliage clumping index using multi-angular satellite data," *Remote Sens. Environ.*, vol. 97, no. 4, pp. 447–457, Sep. 2005.

[33] W. Lucht, C. B. Schaaf, and A. H. Strahler, "An algorithm for the retrieval of albedo from space using semiempirical BRDF models," *IEEE Trans. Geosci. Remote Sens.*, vol. 38, no. 2, pp. 977–998, Mar. 2000.

[34] L. He, J. M. Chen, J. Pisek, C. B. Schaaf, and A. H. Strahler, "Global clumping index map derived from the MODIS BRDF product," *Remote Sens. Environ.*, vol. 119, pp. 118–130, Apr. 2012.

[35] J. M. Chen, A. Govind, O. Sonnentag, Y. Zhang, A. Barr, and B. Amiro, "Leaf area index measurements at fluxnet-Canada forest sites," *Agric. For. Meteorol.*, vol. 140, nos. 1–4, pp. 257–268, Nov. 2006.

[36] C. Coursolle, H. A. Margolis, A. G. Barr, T. A. Black, B. D. Amiro, J. H. McCaughey, L. B. Flanagan, P. M. Lafleur, N. T. Roulet, C. P. A. Bourque, M. A. Arain, S. C. Wofsy, A. Dunn, K. Morgenstern, A. L. Orchansky, P. Y. Bernier, J. M. Chen, J. Kidston, N. Saigusa, and N. Hedstrom, "Late-summer carbon fluxes from Canadian forests and peatlands along an east-west continental transect," *Can. J. For. Res.*, vol. 36, no. 3, pp. 783–800, Mar. 2006.

[37] J. M. Chen, G. Pavlic, L. Brown, J. Cihlar, S. G. Leblanc, H. P. White, R. J. Hall, D. R. Peddle, D. J. King, J. A. Trofymow, E. Swift, J. Van der Sanden, and P. K. E. Pellikka, "Derivation and validation of Canada-wide coarse-resolution leaf area index maps using high-resolution satellite imagery and ground measurements," *Remote Sens. Environ.*, vol. 80, no. 1, pp. 165–184, Apr. 2002.

[38] J. T. Morisette, J. L. Privette, and C. O. Justice, "A framework for the validation of MODIS land products," *Remote Sens. Environ.*, vol. 83, nos. 1–2, pp. 77–96, Nov. 2002.

[39] J. M. Chen, "Optically-based methods for measuring seasonal variation of leaf area index in boreal conifer stands," *Agric. For. Meteorol.*, vol. 80, nos. 2–4, pp. 135–163, Jul. 1996.

[40] C. J. Kucharik, J. M. Norman, and S. T. Gower, "Measurements of branch area and adjusting leaf area index indirect measurements," *Agric. For. Meteorol.*, vol. 91, nos. 1–2, pp. 69–88, May 1998.

[41] A. G. Barr, T. A. Black, E. H. Hogg, N. Kljun, K. Morgenstern, and Z. Nesic, "Inter-annual variability in the leaf area index of a boreal aspen-hazelnut forest in relation to net ecosystem production," *Agric. For. Meteorol.*, vol. 126, nos. 3–4, pp. 237–255, Nov. 2004.

[42] R. A. Fernandes, A. Abduelgasim, L. Sylvain, S. K. Khurshid, and C. Butson, "Leaf area index maps at 30-m resolution," Oak Ridge Nat. Laboratory Distributed Active Archive Center, Tech. Rep., 2005.

[43] R. Fernandes and S. G. Leblanc, "Parametric (modified least squares) and non-parametric (Theil-Sen) linear regressions for predicting bio-physical parameters in the presence of measurement errors," *Remote Sens. Environ.*, vol. 95, no. 3, pp. 303–316, Apr. 2005.

[44] N. V. Shabanov, D. Huang, W. Yang, B. Tan, Y. Knyazikhin, R. B. Myneni, D. E. Ahl, S. T. Gower, A. R. Huete, L. E. O. C. Aragao, and Y. E. Shimabukuro, "Analysis and optimization of the MODIS leaf area index algorithm retrievals over broadleaf forests," *IEEE Trans. Geosci. Remote Sens.*, vol. 43, no. 8, pp. 1855–1865, Aug. 2005.

[45] R. B. Myneni, R. R. Nemani, and S. W. Running, "Estimation of global leaf area index and absorbed par using radiative transfer models," *IEEE Trans. Geosci. Remote Sens.*, vol. 35, no. 6, pp. 1380–1393, Nov. 1997.

[46] A. Gonsamo, "Leaf area index retrieval using gap fractions obtained from high resolution satellite data: Comparisons of approaches, scales and atmospheric effects," *Int. J. Appl. Earth Obs.*, vol. 12, no. 4, pp. 233–248, Aug. 2010.

[47] R. B. Myneni, Y. Knyazikhin, J. L. Privette, J. Glassy, Y. Tian, Y. Wang, X. Song, Y. Zhang, G. R. Smith, A. Lotsch, M. Friedl, J. T. Moriestte, P. Votava, R. R. Nemani, and S. W. Running, "Global products of vegetation leaf area and fraction absorbed PAR from year one of MODIS data," *Remote Sens. Environ.*, vol. 83, noS. 1–2, pp. 214–231, Feb. 2002.

[48] W. J. Chen, J. Chen, J. Liu, and J. Cihlar, "Approaches for reducing uncertainties in regional forest carbon balance," *Global Biogeochem. Cycles*, vol. 14, no. 3, pp. 827–838, Sep. 2000.

[49] J. Liu, J. M. Chen, J. Cihlar, and W. M. Park, "A process-based boreal ecosystem productivity simulator using remote sensing inputs," *Remote Sens. Environ.*, vol. 62, no. 2, pp. 158–175, Nov. 1997.

Jing M. Chen received the B.Sc. degree in applied meteorology from the Nanjing Institute of Meteorology, Nanjing, China, in 1982, and the Ph.D. degree in meteorology from Reading University, Reading, U.K., in 1986.

He was a Postdoctoral Fellow and Research Associate with the University of British Columbia, Vancouver, BC, Canada, from 1989 to 1993. From 1993 to 2000, he was a Research Scientist with the Canada Centre for Remote Sensing, Ottawa, ON, Canada. He is currently a Professor with the University of Toronto, Toronto, ON, and an Adjunct Professor with York University, Toronto. He has authored over 200 papers in refereed journals. His current research interests include the remote sensing of biophysical parameters, plant canopy radiation modeling, terrestrial water and carbon cycle modeling, and atmospheric inverse modeling for global and regional carbon budget estimation.

Dr. Chen is a Fellow of the Royal Society of Canada and a Senior Canada Research Chair. He served as an Associate Editor of the IEEE TRANSACTIONS ON GEOSCIENCE AND REMOTE SENSING from 1996 to 2002.

Alemu Gonsamo studied forestry at Wondo Genet College of Forestry, Debub University, Ethiopia. He received the B.Sc. degree (great distinction) in 2002, the M.Sc. degree in geo-information science from Wageningen University, Wageningen, The Netherlands, in 2006, and the Ph.D. degree in geography from the University of Helsinki, Helsinki, Finland, in 2010.

He was a Graduate Assistant and Academic Coordinator from 2002 to 2004. In 2010, he was a Postdoctoral Fellow with the Department of Geography and Geosciences. He is currently a Postdoctoral Fellow with the University of Toronto, Toronto, ON, Canada. His current research interests include the remote sensing of bio-geophysical parameters, plant canopy radiation modeling, optical satellite sensor cross calibration, remote sensing of land surface phenology, and territorial carbon cycle modeling.